# Extracellular filaments revealed by affinity capture cryo-electron tomography of lymphocytes

**Leeya Engel**[1, 2, ✉], **Magda Zaoralova**[1], **Alexander R. Dunn**[1], **and Stefan Oliver**[3,✉]

[1]Department of Chemical Engineering, Stanford University, Stanford, CA, USA 94305
[2]Faculty of Mechanical Engineering, Technion - Israel Institute of Technology, Haifa, Israel 3200003
[3]Department of Pediatrics, Division of Infectious Diseases, Stanford School of Medicine, Biomedical Innovations 240 Pasteur Drive, Stanford, CA, USA 94305

**Cryogenic-electron tomography (cryo-ET) has provided an unprecedented glimpse into the nanoscale architecture of cells by combining cryogenic preservation of biological structures with electron tomography. Micropatterning of extracellular matrix proteins is increasingly used as a method to prepare adherent cell types for cryo-ET as it promotes optimal positioning of cells and subcellular regions of interest for vitrification, cryo-focused ion beam (cryo-FIB) milling, and data acquisition. Here we demonstrate a micropatterning workflow for capturing minimally adherent cell types, human T-cells and Jurkat cells, for cryo-FIB and cryo-ET. Our affinity capture system facilitated the nanoscale imaging of Jurkat cells, revealing extracellular filamentous structures. It improved workflow efficiency by consistently producing grids with a sufficient number of well-positioned cells for an entire cryo-FIB session. Affinity capture can be extended to facilitate high resolution imaging of other adherent and non-adherent cell types with cryo-ET.**

**cryo-EM | cryo-ET | Jurkat cells | micropatterning | lymphocytes**
**Correspondence:** ***sloliver@stanford.edu, leeya@technion.ac.il***

DRAFT

## Introduction

Cryogenic-electron tomography (cryo-ET) is a state-of-the-art electron microscopy (EM) modality used for the structural analysis of intact, vitrified cells at the nanometer and subnanometer scales (1–6). In preparation for cryo-ET, cells are deposited or grown on specialized substrates called EM grids. To image eukaryotic cells, which are on the length scale of micrometers, thinning the cells using techniques such as cryo-focused ion beam (cryo-FIB) milling is typically required. Cells tend to distribute in a nonuniform manner on EM grids, and settle on the metal grid bars where they are not accessible for cryo-FIB and cryo-ET. In addition, cells can form clumps that prevent proper vitrification and successful FIB milling. These limitations present an obstacle both to the collection of cryo-ET data of sufficient quality from biological specimens and to the automation of data collection and cryo-FIB milling.

To gather sufficient data for high resolution structural determination, reproducible samples are needed. Time on high-end cryo-FIB and cryo-ET instrumentation, typically accessed through shared cryo-EM facilities, is limited. An ideal sample for cryo-FIB/cryo-ET would have a repeatable and uniform distribution of cells situated in the centers of the grid squares. We and others have published studies demonstrating the positioning of individual adherent cells (7–11) or adherent cell pairs (12, 13) on EM grids micropatterned with extracellular matrix (ECM) proteins in preparation for cryo-ET. Another approach for providing a uniform distribution of cells for cryo-FIB/cryo-ET, applicable to both adherent and non-adherent cell types, is the Waffle Method (14). It employs high pressure freezing to vitrify a contained, continuous suspension of cells in preparation for cryo-FIB/cryo-ET. High pressure freezing, however, can be technically challenging and results in thicker samples (10s of microns) that require extended cryo-FIB milling times.

Lymphocytes (e.g., T-cells and B-cells) are minimally adherent cells that play important roles in the body's defense against infectious diseases and cancer. Recent advances in our understanding of lymphocyte function have been provided by fluorescence imaging and conventional EM (15, 16). However, the resolution of fluorescence imaging is limited by the wavelength of light and conventional EM techniques require fixation and staining steps that can distort or destroy delicate biological structures.

Here we present an affinity capture system that facilitates high throughput cryo-FIB milling and subsequent nanoscale imaging by cryo-ET of non-adherent cell types that is compatible with vitrification by plunge-freezing. We micropatterned antibodies (Abs) on EM grids to capture T-cells as well as Jurkat cells, an immortalized line of human T lymphocytes, and position them in the centers of EM grid squares. This facilitated our observation of nanoscale filaments emanating from the Jurkat cells. To our knowledge, this is the first time that micropatterning has been used to prepare minimally adherent cell types for cryo-ET.

## Results

To assess the feasibility of capturing non-adherent cell lines on EM grids, a T-cell specific antibody to human CD3 (epsilon chain) was micropatterned to trap the T-cell surrogate, Jurkat cells, on islands within grid squares. Affinity capture grids were able to successfully capture single Jurkat cells and position them in the centers of the grid squares (Fig. 1A-C, S1, S2). Cell localization was restricted to the micropatterned region on EM grids treated with the anti-CD3 antibody (Fig.

1B and 1C). Neither of the control conditions, micropatterned grids without Ab or a nonspecific Ab (gE), contained cells following a PBS rinse (Fig. S1). We were also able to use this workflow to capture and position primary T-cells on EM grids micropatterned with anti-CD3 islands (Fig. S3-S4).

The number of Jurkat cells occupying a given grid square increased with the size of the micropatterned Ab island (Fig. 2). Micropatterned islands that were about half the size of Jurkat cells (i.e., 5 µm) were unable to capture the cells. Circular 10 µm islands of micropatterned anti-CD3 were ideal for vitrification and cryo-FIB/SEM of Jurkat cells (Fig. 1C-F). A typical affinity grid seeded with Jurkat cells contained more well-positioned single cells than can be milled in a typical manual cryo-FIB session (>10) (Fig. 1C, D). The target thickness (175 nm) of individually cryo-FIB milled Jurkat cells was readily achieved (Fig. 1E, F).

Cryo-ET of the cryo-FIB milled lamellae revealed cellular features within and external to the Jurkat cells (Figs. 3, 4, S5, S6). While Jurkat cells had a smooth and round appearance when observed with light microscopy and cryo-SEM (Fig. 1, 2, and 3), extracellular, filamentous structures were discovered in the tomograms reconstructed from the cryo-ET tilt-series (Figs. 3, 4, and movies 1 and 2). These filaments had an external diameter of approximately 10 nm and an apparent internal diameter of approximately 3 nm (Fig. S6). Although the length of the filaments could not be determined, they are likely on the order of micrometers as they traverse the entire field of view within the 3D cryo-tomograms (Fig. 3C). In most regions, the filaments appeared to form a quasi-random network. However, close to the cell surface, and particularly in regions between contacting cells, the filaments appeared to form bundles (Fig. 4A, B). Segmentation of the cryo-tomograms also revealed the nuclear envelope, vesicular structures, and plasma membrane.

## Discussion

We have demonstrated an affinity capture system for positioning non-adherent cell types for cryo-FIB milling and cryo-ET. T-cells have been observed in the literature to form stable attachments to micropatterned islands of CD3 antibodies on glass surfaces (17). Thus, this is the likely mechanism of affinity capture.

Affinity capture grids facilitated our observation of nanoscale filaments on the surface of Jurkat cells (Figs. 3-4). It is possible that this filamentous surface coating represents the glycocalyx (18). Similarly structured filamentous networks were recently observed in the enteric glycocalyx using freeze-etching electron tomography (19). Based on their size, it is also conceivable that the filamentous network is comprised of keratin (20, 21). However, intermediate filaments are typically intracellular structures. Further data collection combined with subtomogram averaging would be required to definitively determine the identity of the filaments.

Jurkat cells have been observed to shed microvillus particles on anti-CD3 treated surfaces using total internal reflection fluorescence microscopy (TIRF) (16), but not individual filaments such as those that appear in our cryo-tomograms (Figs. 3C and 4D), likely because these structures are too small (10 nm) to be observed by fluorescence microscopy. The filaments were also not observed by conventional transmission and scanning EM (TEM and SEM) imaging of the Jurkat cell surface (16). While these EM modalities can provide higher resolution than light microscopy, conventional EM requires preparation steps that would likely cause the collapse of delicate structures such as networks of filaments on the cell surface. Specifically, for conventional SEM of cells, preparation steps include fixation, dehydration, and the deposition of a conductive metal layer. For conventional TEM, preparation of cells includes fixation, dehydration, resin embedding, staining, and sectioning. Cryo-ET overcomes the limitations of these destructive processing methods, providing the highest resolution imaging of cells preserved in a hydrated, near-native state. In our cryo-FIB/ET study, preservation of nanoscale biological structures through vitrification converged with image processing techniques to provide an unprecendented view of the nanoscale environment of the Jurkat cell surface. Other recent studies have demonstrated the power of the cryo-FIB/cryo-ET platform to reveal additional complexity to biological structures such as microvilli despite decades of structural analysis by conventional EM (22). We envision the workflow presented here facilitating future analysis of the nanoscale structures involved in T-cell activation.

The affinity capture system improves sample usability, reducing the cost and preparation time required to prepare cellular samples for cryo-FIB/ET. Beyond positioning cells and limiting the number of cells that attach to a given region of the substrate, the use of micropatterned islands functionalized with antibodies, ligands, and ECM proteins can potentially be extended to select for and capture cell types of interest from diverse cell populations. Alternatively, two different antibodies can potentially be patterned to capture different cell types within the same grid square for co-culture studies. Patterns comprised of different ligands can also be used to study how the spatial organization of signaling complexes impacts the structures involved in cell communication (17), such as receptor arrangement (23). An extension of this idea is to facilitate studies of the nanoscale architectures involved in cell-cell interactions such as signaling events or the growth and structure of nanoscale bridges by systematically varying the distance between captured cells using micropatterns, such as the diamond configuration that we produced in Fig. S7.

Appropriately packaged affinity capture EM grids could assist non-experts (e.g., clinicians lacking EM experience) with preparing and shipping clinically-relevant cells to cryo-EM facilities for imaging. Packaging methods currently include the use of 3D printed grid holders (24) and silicone wells in glass-bottom dishes that exploit the surface tension of liquid droplets contained to the wells to immobilize EM grids (11). It might be possible to immobilize dry micropatterned grids on silicone pads within sterile dishes to be rehydrated prior to cell culture, but future work is required to test the stability of the anti-fouling PEG coating of the EM grids as a function of the storage environment before this can be implemented. Devising storage methods to increase the shelf life of micropat-

DRAFT

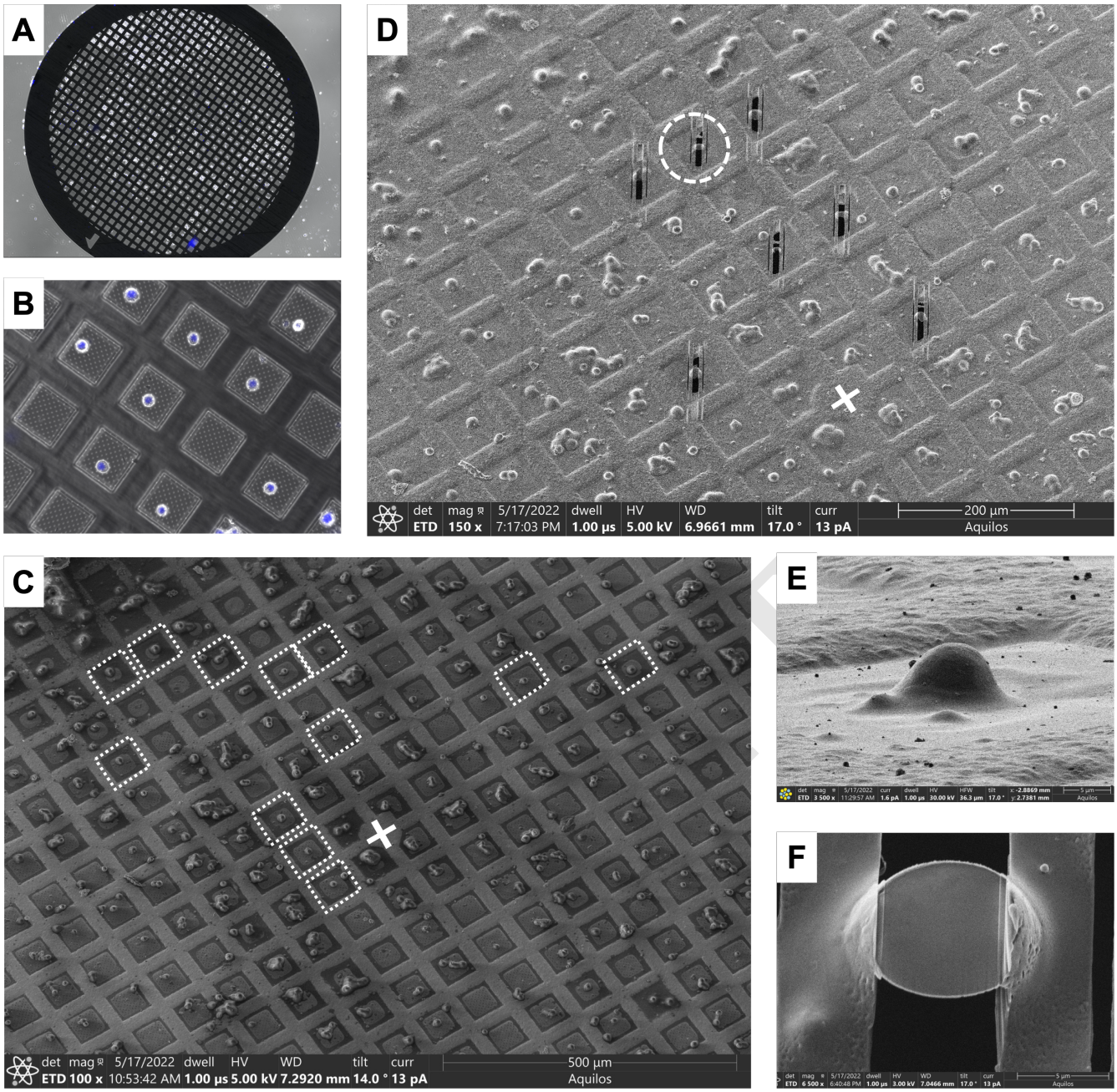


**Fig. 1.** Affinity capture EM grids facilitate cryo-FIB of minimally adherent cells. (A) Fluorescence image overlaid with brightfield image of 300 mesh EM grid micropatterned with 10 µm circles following antibody incubation and cell capture. (B) Close up shows single cells centrally positioned on grid squares (nuclei are in blue). (C) Cryo-SEM image of an EM grid with vitrified cells centrally positioned in grid squares suitable for cryo-FIB (denoted by dotted white squares). The grid center is marked with a white cross. (D) Cryo-SEM image of the EM grid from C after cryo-FIB milling of seven Jurkat cells, with the grid center marked with a white cross. As is typical for cryo-FIB, all milled cells are north of the grid center. (E) Ion beam image of cell selected for cryo-FIB milling, indicated in D by the white dotted circle. (E and F) A platinum-coated Jurkat cell (E) and a lamella generated from the cell after cryo-FIB milling (F).

terned EM grids is an important future area of research for increasing access to and utility of affinity capture EM grids.

## Methods

**EM grid micropatterning.** To accommodate single Jurkat cells, we micropatterned squares and circles varying from 5 to 30 µm across on 300 mesh gold grids coated with a thin perforated layer of silicon dioxide (Quantifoil R1/4). The grids were exposed to atmospheric plasma, incubated in poly-l-lysine (PLL, Sigma cat # p4707), incubated in mPEG-Succinimidyl Valerate, MW 5,000 (PEG-SVA, Laysan Bio Inc) and then UV exposed according to digitally generated micropatterns using the Primo photo-micropatterning system (Alveole) to selectively degrade the PEG coating on the EM grids. A detailed protocol for micropatterning EM grids using this method has been made publicly available by the authors on the protocol sharing platform protocols.io (11).

Following micropatterning of the grids and sterilization in 70% ethanol (see aforementioned protocol), the grids were incubated in human anti-CD3 (clone UCHT1; Biolegend

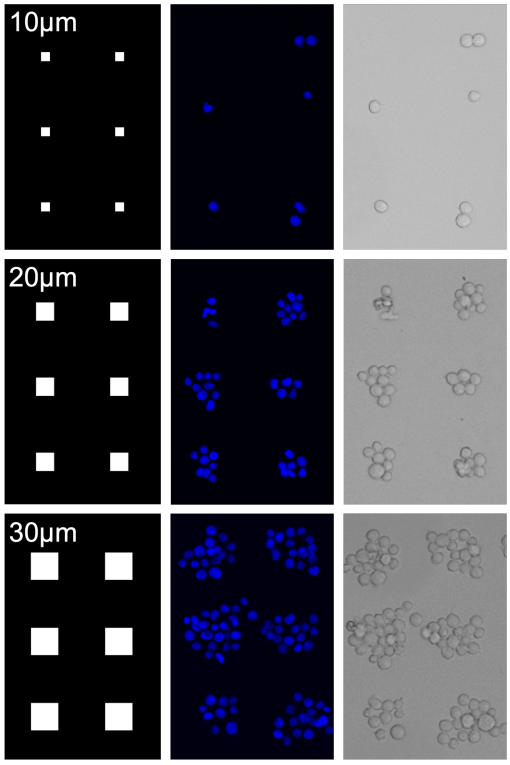


**Fig. 2.** Cell occupancy increases with larger micropatterned anti-CD3 islands. Examples of micropatterned squares with side lengths ranging from from 10 µm to 30 µm. Left panel: digital micropatterns designed to match the pitch of a 300 mesh EM grid. Jurkat cells attached to micropatterned glass incubated with an anti-CD3 mAb. DAPI (middle panel), brightfield (right panel).

Cat# 300402) antibody overnight. Control conditions included a set of micropattterned grids that were not incubated in antibody (No Ab) and another set of micropatterned grids that were treated with monoclonal antibodies to VZV glycoprotein E (gE; EMD Millipore Cat# MAB8612).

For T-cells, 200 mesh gold Quantifoil holey carbon R2,2 grids were micropatterned followed the same protocol, but with micropatterned circles that were 7.5 and 15 µm in diameter.

**Jurkat cell culture and seeding.** Jurkat cells (Jurkat, Clone E6-1, ATCC) were maintained following manufacturer instructions. A volume of 10 µL of a 7x$10^6$ cells/mL suspension was seeded on the micropatterned grids and allowed to settle for two hours. The grids were then transferred to fresh 35 mm dishes with 10 mm 1.5 cover glass (MatTek) and washed extensively with media (RPMI 1640 + 10% FBS + 1% pen/strep). The grids were then washed once with 2 mL PBS, fixed in 1 mL 4% PFA, and washed twice with 2 mL PBS.

Prior to imaging, the PBS was aspirated and replaced with 2 mL PBS plus 1:1000 Hoechst 33342 to stain the cell nuclei. Images were captured with a BZ-X710 microscope (Keyence). Brightness and contrast in Fig. 2 were adjusted to improve visibility.

**T-cell culture and seeding.** Human T-cells (gift from Robbie Majzner's lab at Stanford University) were purified from isolated peripheral blood mononuclear cells as in Tousley et al. (25). They were maintained in AIM-V complete media (Gibco) supplemented with 5% FBS and IL-2 (2.18 IU/ng, Peprotech). To seed the cells on the micropatterned grids, 25 uL of a 4x$10^5$ cell/mL suspension was added to each grid several times until we could observe approximately 2-3 cells above or on each grid square. Images of live T-cells on micropatterned Au 200 mesh holey carbon coated EM grids were captured after 5.5 hrs on an inverted Nikon Ti-E microscope (Nikon, Minato, Tokyo, Japan) equipped with a Heliophor light engine (89 North) and an Andor sCMOS Neo camera using a 20x Plan Apo Lambda air objective lens and a 60x Plan Apo Lambda oil objective lens. The samples were vitrified by plunge freezing.

**Vitrification and cryo-FIB.** Samples were vitrified in a Leica EM GP plunge freezer and clipped into autogrids before being loaded into an Aquilos 2 (Thermo Fisher) for cryo-FIB milling. Lamella were cryo-FIB milled at a 10 degree milling angle first to a 5 µm thickness with a current of 1 nA. Microexpansion joints were cryo-FIB milled to prevent bending and breaking of the cryo-lamellae (26). Sequential milling was performed at 0.3 nA to 3 µm thickness, at 100 pA to 1um thickness, and at 50 pA to 500 nm thickness. A final polish was performed with a 175 nm distance between rectangular patterns at a current of 30 pA.

**Cryo-ET data acquisition and tomogram reconstruction.** Samples were loaded into an FEI Krios G2 transmission electron microscope (TEM) equipped with a bioquantum energy filter and a K3 direct electron detector (Gatan). SerialEM software (27) was used to operate the TEM at 300 kV in low-dose mode and acquire tilt series at a magnification 26,000x (0.3366 nm/pixel). Tilt series were acquired with $2^o$ steps between -$60^o$ and +$60^o$ and a defocus of -4 µm. Motion correction was performed with MotionCor2 software (28) and 3D reconstructions were calculated using the weighted-back projection using IMOD (29). AI segmentation of tomograms was performed using the Dragonfly (Version 2022.2.0.1367; Object Research Systems) Deep Learning Tool. UCSF Chimera was used for visualization of structures (30).

**ACKNOWLEDGEMENTS**

This work was supported by NIH R01 AI20459 (SO), R21 AI159375 (SO), R35 GM130332 (ARD), and a Diane and Guilford Glazer Foundation Faculty Fellowship (LE). We thank and Eva de la Serna (Dunn lab) for culturing the T-cells on micropatterned EM grids. We thank Dr. Lydia-Marie Joubert for providing cryo-FIB training, experimental support, and for helpful feedback. We thank Dr. Matthew J. Paszek (Cornell) for helpful discussion. We thank the Stanford Cryo-Electron Microscopy Center (cEMc) for providing access to a Krios cryo-TEM for data collection. Cryo-FIB for this work was performed at the Stanford-SLAC CryoET Specimen Preparation Center (SCSC), which is supported by the National Institutes of Health Common Fund's Transformative High Resolution Cryoelectron Microscopy program (U24GM139166). The content is solely the responsibility of the authors and does not necessarily represent the official views of the National Institutes of Health. This manuscript was prepared using the Henriques lab bioRxiv template on Overleaf. The authors declare no competing financial interests.

## Author Contributions

LE: Conceptualization, Methodology, Validation, Investigation, Writing - Original Draft, Visualization, Supervision,

DRAFT

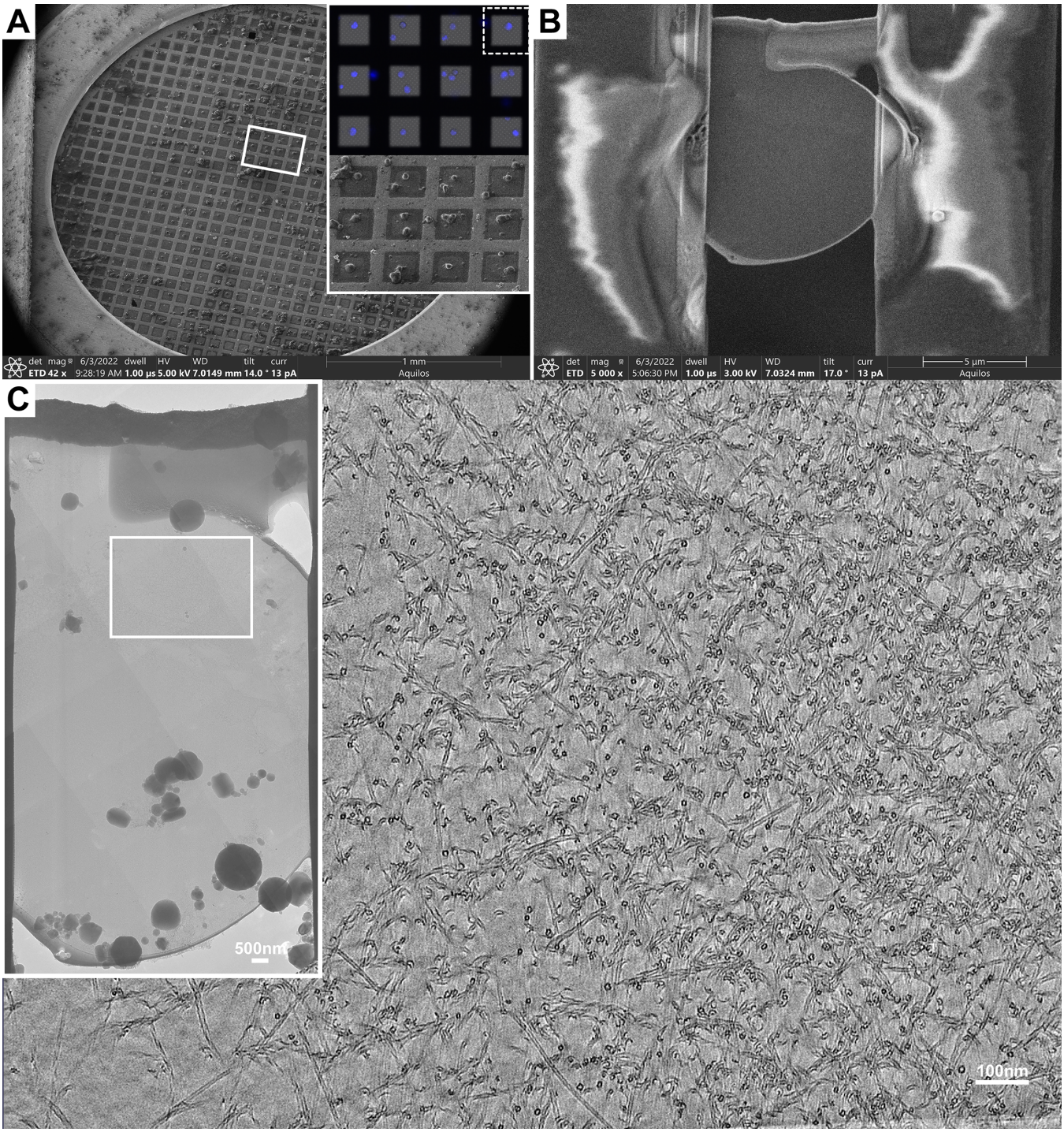


**Fig. 3.** Cryo-FIB/cryo-ET identifies filaments emanating from Jurkat cells on affinity captured grids. (A) Cryo-SEM of cells vitrified on an affinity capture grid micropatterned with 10 µm circles. Inset shows live-cell fluorescence micrograph of nuclei stained with Hoechst 33342 as well as a close up on the SEM image. (B) A lamella produced from a Jurkat cell via cryo-FIB milling with an Aquilos2. The lamella was produced from the cell highlighted by the dotted box of the inset in panel A. (C) Cryo-ET of the lamella from panel B. The inset shows a medium magnification (8,700X) montage of the lamella. The white box highlights the area where a tilt series was collected to produce a cryo-tomogram; a single slice is shown (see Suppl. Movie 1 for the entire tomogram).

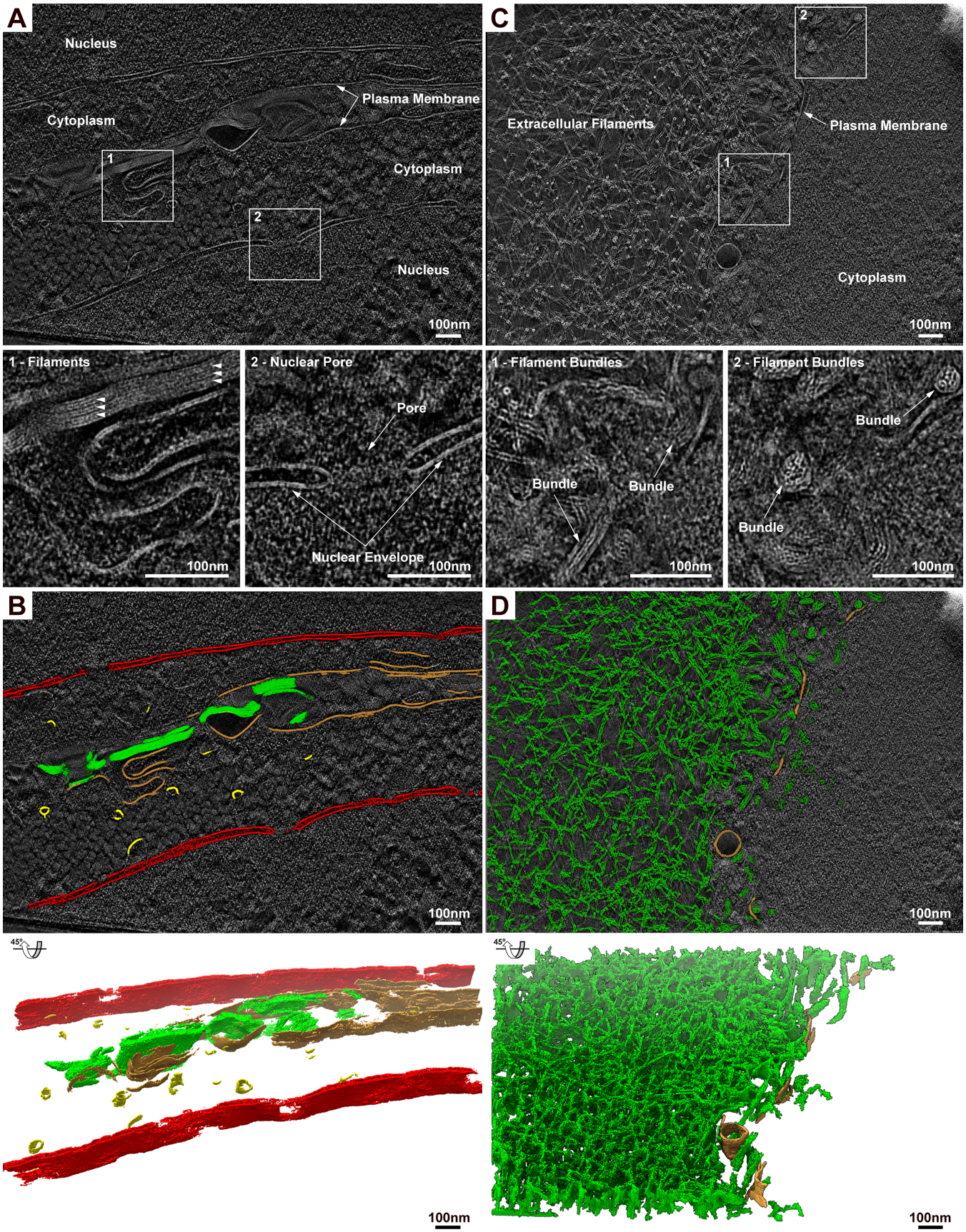


**Fig. 4.** Affinity capture grids facilitate the visualization of nanoscale structures at the plasma membrane of Jurkat cells via *in situ* cryo-ET. (A to D) Tomogram reconstructions and AI-based segmentation of cryo-FIB milled Jurkat cells. (A) Cryo-tomographic slice of the region between adjacent cells showing (1) bundled filaments and (2) a nuclear pore. (C) Cryo-tomographic slice showing extracellular filaments. In the region closer to the plasma membrane filament bundles can be seen from the side (1) and in cross section (2). (B and D) AI-based segmentation of filaments (green), plasma membrane (brown), vesicles (yellow), and nuclear envelope (red) identified in the tomograms for panels A and B. (See Suppl. Movie 2 for full tomograms and Figure S5 for lower magnification images of corresponding cells and lamellae.) All scale bars are 100 nm.

Project administration. MZ: Investigation, Writing - Review & Editing. ARD: Resources, Writing - Review & Editing, Supervision, Funding acquisition. SO: Conceptualization, Methodology, Software, Validation, Formal analysis, Investigation, Resources, Data Curation, Writing - Original Draft, Visualization, Supervision, Project administration, Funding acquisition.

## Bibliography


1. Ohad Medalia, Igor Weber, Achilleas S Frangakis, Daniela Nicastro, Günther Gerisch, and Wolfgang Baumeister. Macromolecular architecture in eukaryotic cells visualized by cryo-electron tomography. *Science*, 298(5596):1209–1213, 2002.
2. Shoh Asano, Benjamin D Engel, and Wolfgang Baumeister. In situ cryo-electron tomography: a post-reductionist approach to structural biology. *Journal of molecular biology*, 428 (2):332–343, 2016.
3. Lu Gan and Grant J Jensen. Electron tomography of cells. *Quarterly reviews of biophysics*, 45(1):27–56, 2012.
4. Saikat Chakraborty, Marion Jasnin, and Wolfgang Baumeister. Three-dimensional organization of the cytoskeleton: a cryo-electron tomography perspective. *Protein Science*, 2020.
5. Vladan Lučić, Friedrich Förster, and Wolfgang Baumeister. Structural studies by electron tomography: from cells to molecules. *Annu. Rev. Biochem.*, 74:833–865, 2005.
6. Stephan Nickell, Christine Kofler, Andrew P Leis, and Wolfgang Baumeister. A visual approach to proteomics. *Nature reviews Molecular cell biology*, 7(3):225–230, 2006.
7. Leeya Engel, Guido Gaietta, Liam P Dow, Mark F Swif, Gaspard Pardon, Niels Volkmann, William I Weis, Dorit Hanein, and Beth L Pruitt. Extracellular matrix micropatterning technology for whole cell cryogenic electron microscopy studies. *Journal of Micromechanics and Microengineering*, 29(11):115018, 2019.
8. Mauricio Toro-Nahuelpan, Ievgeniia Zagoriy, Fabrice Senger, Laurent Blanchoin, Manuel Théry, and Julia Mahamid. Tailoring cryo-electron microscopy grids by photo-micropatterning for in-cell structural studies. *Nature methods*, 17(1):50–54, 2020.
9. Léa Swistak, Anna Sartori-Rupp, Matthijn Vos, and Jost Enninga. Micropatterning of cells on em grids for efficient cryo-correlative light electron microscopy. In *Methods in Microbiology*, volume 48, pages 95–110. Elsevier, 2021.
10. Bryan S Sibert, Joseph Y Kim, Jie E Yang, and Elizabeth R Wright. Micropatterning transmission electron microscopy grids to direct cell positioning within whole-cell cryo-electron tomography workflows. *Journal of visualized experiments: JoVE*, (175), 2021.
11. Leeya Engel, Richard Held, Claudia G Vasquez, William I Weis, and Alexander R Dunn. Micropatterning em grids for cryo-electron tomography of cells. *protocols.io*, page dx.doi.org/10.17504/protocols.io.bz22p8ge, 2022.
12. Leeya Engel, Claudia G Vasquez, Elizabeth A Montabana, Belle M Sow, Marcin P Walkiewicz, William I Weis, and Alexander R Dunn. Lattice micropatterning for cryo-electron tomography studies of cell-cell contacts. *Journal of structural biology*, 213(4):107791, 2021.
13. Liam P Dow, Guido Gaietta, Yair Kaufman, Mark F Swift, Moara Lemos, Kerry Lane, Matthew Hopcroft, Armel Bezault, Cécile Sauvanet, Niels Volkmann, et al. Morphological control enables nanometer-scale dissection of cell-cell signaling complexes. *Nature Communications*, 13(1):7831, 2022.
14. Kotaro Kelley, Ashleigh M Raczkowski, Oleg Klykov, Pattana Jaroenlak, Daija Bobe, Mykhailo Kopylov, Edward T Eng, Gira Bhabha, Clinton S Potter, Bridget Carragher, et al. Waffle method: A general and flexible approach for improving throughput in fib-milling. *Nature Communications*, 13(1):1857, 2022.
15. Jane C Stinchcombe, Yukako Asano, Christopher JG Kaufman, Kristin Böhlig, Christopher J Peddie, Lucy M Collinson, André Nadler, and Gillian M Griffiths. Ectocytosis renders t cell receptor signaling self-limiting at the immune synapse. *Science*, 380(6647):818–823, 2023.
16. Hye-Ran Kim, YeVin Mun, Kyung-Sik Lee, Yoo-Jin Park, Jeong-Su Park, Jin-Hwa Park, Bu-Nam Jeon, Chang-Hyun Kim, Youngsoo Jun, Young-Min Hyun, et al. T cell microvilli constitute immunological synaptosomes that carry messages to antigen-presenting cells. *Nature Communications*, 9(1):3630, 2018.
17. Keyue Shen, V Kaye Thomas, Michael L Dustin, and Lance C Kam. Micropatterning of costimulatory ligands enhances cd4+ t cell function. *Proceedings of the National Academy of Sciences*, 105(22):7791–7796, 2008.
18. S Ito. Form and function of the glycocalyx on free cell surfaces. *Philosophical Transactions of the Royal Society of London. B, Biological Sciences*, 268(891):55–66, 1974.
19. Willy W Sun, Evan S Krystofiak, Alejandra Leo-Macias, Runjia Cui, Antonio Sesso, Roberto Weigert, Seham Ebrahim, and Bechara Kachar. Nanoarchitecture and dynamics of the mouse enteric glycocalyx examined by freeze-etching electron tomography and intravital microscopy. *Communications biology*, 3(1):5, 2020.
20. Zhikai Wang, Philip Moresco, Ran Yan, Jiayun Li, Ya Gao, Daniele Biasci, Min Yao, Jordan Pearson, Jaclyn F Hechtman, Tobias Janowitz, et al. Carcinomas assemble a filamentous cxcl12–keratin-19 coating that suppresses t cell–mediated immune attack. *Proceedings of the National Academy of Sciences*, 119(4):e2119463119, 2022.
21. Oluseye Ogunnigbagbe, Christopher G Bunick, and Kamaljit Kaur. Keratin 1 as a cell-surface receptor in cancer. *Biochimica et Biophysica Acta (BBA)-Reviews on Cancer*, 1877 (1):188664, 2022.
22. Hao Zhu, Meijing Li, Ruixue Zhao, Ming Li, Yongping Chai, Zhiwen Zhu, Yihong Yang, Wei Li, Zhongyun Xie, Xiaomin Li, et al. In situ structure of intestinal apical surface reveals nanobristles on microvilli. *Proceedings of the National Academy of Sciences*, 119 (24):e2122249119, 2022.
23. Guillaume Le Saux, Esti Toledo-Ashkenazi, and Mark Schvartzman. Fabrication of nanoscale arrays to study the effect of ligand arrangement on inhibitory signaling in nk cells. In *The Immune Synapse: Methods and Protocols*, pages 313–325. Springer, 2023.
24. Florian Fäßler, Bettina Zens, Robert Hauschild, and Florian KM Schur. 3d printed cell culture grid holders for improved cellular specimen preparation in cryo-electron microscopy. *Journal of Structural Biology*, 212(3):107633, 2020.
25. Aidan M Tousley, Maria Caterina Rotiroti, Louai Labanieh, Lea Wenting Rysavy, Won-Ju Kim, Caleb Lareau, Elena Sotillo, Evan W Weber, Skyler P Rietberg, Guillermo Nicolas Dalton, et al. Co-opting signalling molecules enables logic-gated control of car t cells. *Nature*, pages 1–10, 2023.
26. Georg Wolff, Ronald WAL Limpens, Shawn Zheng, Eric J Snijder, David A Agard, Abraham J Koster, and Montserrat Bárcena. Mind the gap: Micro-expansion joints drastically decrease the bending of fib-milled cryo-lamellae. *Journal of structural biology*, 208(3):107389, 2019.
27. David N Mastronarde. Automated electron microscope tomography using robust prediction of specimen movements. *Journal of structural biology*, 152(1):36–51, 2005.
28. Shawn Q Zheng, Eugene Palovcak, Jean-Paul Armache, Kliment A Verba, Yifan Cheng, and David A Agard. Motioncor2: anisotropic correction of beam-induced motion for improved cryo-electron microscopy. *Nature methods*, 14(4):331–332, 2017.
29. James R Kremer, David N Mastronarde, and J Richard McIntosh. Computer visualization of three-dimensional image data using imod. *Journal of structural biology*, 116(1):71–76, 1996.
30. Eric F Pettersen, Thomas D Goddard, Conrad C Huang, Elaine C Meng, Gregory S Couch, Tristan I Croll, John H Morris, and Thomas E Ferrin. Ucsf chimerax: Structure visualization for researchers, educators, and developers. *Protein Science*, 30(1):70–82, 2021.


DRAFT